Biosensors and Bioelectronics 62 (2014) 25–30

Contents lists available at ScienceDirect

Biosensors and Bioelectronics

journal homepage: www.elsevier.com/locate/bios

An electrochemical ELISA-like immunosensor for miRNAs detection based on screen-printed gold electrodes modified with reduced graphene oxide and carbon nanotubes

H.V. Tran [a,b,d], B. Piro [a], S. Reisberg [a], L. Huy Nguyen [a], T. Dung Nguyen [a], H.T. Duc [c], M.C. Pham [a,*]

[a] Université Paris Diderot, Sorbonne Paris Cité, ITODYS, UMR 7086 CNRS, 15 rue J-A de Baïf, 75205 Paris Cedex 13, France
[b] USTH, University of Science and Technology of Hanoi, 18 Hoang Quoc Viet, Hanoi, Vietnam
[c] Université Paris 11, INSERM U-1014, Hôpital Paul Brousse 94800 Villejuif, France
[d] School of Chemical Engineering, Hanoi University of Science and Technology, 1st Dai Co Viet Road, Hanoi, Vietnam

ARTICLE INFO

Article history:
Received 17 March 2014
Received in revised form
6 June 2014
Accepted 10 June 2014
Available online 14 June 2014

Keywords:
Reduced graphene oxide
Carbon nanotubes
Electrochemical biosensor
Label-free detection
miRNA
Immunodetection

ABSTRACT

We design an electrochemical immunosensor for miRNA detection, based on screen-printed gold electrodes modified with reduced graphene oxide and carbon nanotubes. An original immunological approach is followed, using antibodies directed to DNA.RNA hybrids. An electrochemical ELISA-like amplification strategy was set up using a secondary antibody conjugated to horseradish peroxidase (HRP). Hydroquinone is oxidized into benzoquinone by the HRP/H_2O_2 catalytic system. In turn, benzoquinone is electroreduced into hydroquinone at the electrode. The catalytic reduction current is related to HRP amount immobilized on the surface, which itself is related to miRNA.DNA surface density on the electrode. This architecture, compared to classical optical detection, lowers the detection limit down to 10 fM. Two miRNAs were studied: miR-141 (a prostate biomarker) and miR-29b-1 (a lung cancer biomarker).

1. Introduction

Graphene (GR) is considered as one of the most important materials nowadays. Its high specific area makes it excellent platform for biosensors, nanodevices or drug delivery (Chen et al., 2012; Dong et al., 2011; Feng et al., 2012; Georgakilas et al., 2012; Hu et al., 2012). However, graphene is very difficult to disperse in most solvents and does not present available functional groups to bind external molecules (e.g. biomolecules), which restricts its applications. On the contrary, graphene oxide (GO) and reduced graphene oxide (RGO), easier to disperse in aqueous or organic solvents, offer better functionalization capabilities: GO and RGO present carbonyl, epoxy, and carboxylic acid groups able to bind molecules through covalent bonds (Dreyer et al., 2010). Many publications have described application of GO and RGO for DNA or peptide detection (previously cited articles, and Wu et al., 2012; Feng et al., 2013; Huang et al., 2012; Dong et al., 2012a). However, miRNAs detection has been less described and mainly based on fluorescence quenching on graphene; few publications investigated electrochemical transduction on these materials (Cui et al., 2012; Yin et al., 2012; Tran et al., 2013a). miRNAs are a class of small non-protein-coding single strand ribonucleic acid molecules (RNAs) of 18 to 30 nucleotides which play crucial roles in cell proliferation, differentiation and apoptosis. The discovery in 2008 that miRNAs are present in body fluids in correlation with cancers (prostate, breast, colon, lung, ovarian, leukemia, etc.) or other diseases (diabetes, heart diseases, etc.) makes them important biomarkers for early diagnostic. Current methods for miRNA detection, as quantitative reverse transcription polymerase chain reaction (qRT-PCR), Northern blotting and DNA array technology, only partially meet the requirements needed for routine detection. That is why developing miRNA detection and quantification tools is challenging (Dong et al., 2012a; Yang et al., 2009; Yin et al., 2012; Zhang et al., 2009; Tran et al., 2013b; 2014; Fang et al., 2006). To develop highly sensitive miRNA biosensors, e.g. bioanalytical tools able to detect miRNA below the nanomolar level, many strategies based on nanomaterials have been applied, using graphene (Dong et al., 2012a), silicon nanowires (Yang et al., 2009; Zhang et al., 2009), gold nanoparticles (Roy et al., 2011; Yin et al., 2012), silver nanoclusters (Dong et al., 2012b) or conducting polymer/carbon nanotube hybrids (Tran et al., 2013b).

* Corresponding author. Tel.: +33 1 57277223.
E-mail address: mcpham@univ-paris-diderot.fr (M.C. Pham).

http://dx.doi.org/10.1016/j.bios.2014.06.014
0956-5663/

For example, Zhang et al. (2009) have developed a label-free electrochemical biosensor based on silicon nanowires. This sensor is able to detect miRNA with a limit of detection (LOD) of ca. 10 fM. Peng et al. (2010) have reported an miRNA sensor based on miRNA labeled with ruthenium oxide nanoparticles and incubated, for detection, in a mixture of aniline and H_2O_2. The signal is recorded through CV (cyclic voltammetry) or SWV (square wave voltammetry) with a LOD of 2 fM. Fan et al. (2007) have reported detection of miRNA using target-guided formation of conducting polymer nanowires in nanogaps, for a LOD of ca. 5 fM. Tran et al. (2013b) reported a label-free and reagentless electrochemical biosensor for miRNA detection based on a nanostructured poly (5-hydroxy-1,4-naphthoquinone)/carbon nanotube composite, offering quantitative detection for a range of concentrations from 10 fM to 1 nM and a LOD of ca. 8 fM. Yang et al. (2009) and Fang et al. (2009) have developed microelectrodes based on Pt nanostructures for immobilization of DNA–SH probes to detect miRNAs by SWV in phosphate buffer containing redox indicators $[Ru(NH_3)_6]^{3+}$ or $[Fe(CN)_6]^{3-}$. These systems, which imply a reagent added in solution, can detect miRNAs at the aM level. Roy et al. (2011) have developed a microfluidic miRNA biosensor that allows us to detect miRNAs with a LOD of ca. 1 fM. Another strategy for miRNA detection used allosteric molecular beacons and amperometric detection, with a limit of detection of 3.4 pM (Cai et al., 2013). Gao et al. (2013) have reported a label-free miRNA sensor based on deposition of an insulating polymer film, poly(3.3′-dimethoxybenzidine) (PDB) on hybridized miRNA-template using impedimetric detection , that offers a LOD of ca. 2 fM.

An original strategy has been described by Stollar et al. and developed later (Yoshichika and Stollar, 1982; Rudkin and Stollar, 1977; Fliss et al., 1995). The breakthrough consists in using antibodies specifically directed to RNA.DNA hybrids, which can thereafter be exploited for RNA detection through classical Enzyme Linked ImmunoSorbent Assay (ELISA). However, there are very few recent research works mentioning such miRNA detection through immunoassays (Qavi et al., 2011; Dong et al., 2012c; Sípová et al., 2010). In these studies, antibodies bind miRNA.DNA hybrids attached on a surface and, due to their steric hindrance, enhanced the signal for surface plasmon resonance (SPR), silicon microring photonic resonators detection or electrochemical detection (Tran et al., 2013b).

A recent approach uses protein 19 (p19), which is known to specifically bind to miRNA.DNA hybrids (Labib et al., 2013; Ramnani et al., 2013). The binding of protein to miRNA.DNA hybrids, generates steric hindrance on the electrode surface or change in conductivity of carbon nanotubes.

In the present study, we design an electrochemical immunosensor for miRNA detection, using reduced graphene oxide (RGO) and carbon nanotubes (CNTs) composite and electrochemical ELISA-like amplification strategy. A composite of RGO and MWCNTs was drop-casted on electrodes, then oligonucleotide (ODN) capture probes were grafted and complementary miRNA added. Following hybridization, an antibody directed to RNA.DNA hybrids (hybrids designate RNA.DNA double strands, whereas duplexes designate DNA.DNA double strands) was introduced and was shown to bind selectively to the hybrid. After that, an electrochemical ELISA-like amplification step was set up using a secondary antibody conjugated to horseradish peroxidase (HRP). This architecture, compared to classical optical detection, lowers the detection limit down to 10 fM and has never been described in the literature before. The chromophore which is generally used in ELISA experiments was replaced by hydroquinone, well known to be oxidized into benzoquinone by the HRP/H_2O_2 catalytic system. In turn, benzoquinone was electroreduced into hydroquinone on the electrode set at adequate reduction potential. In this case, the catalytic reduction current was related to HRP immobilized on the surface, which itself was related to miRNA.DNA surface density on the electrode (see Graphical Abstract). This approach has never been reported for miRNA detection. Two miRNAs were studied: miR-141 (a prostate biomarker) and miR-29b (a lung cancer biomarker).

2. Experimental

2.1. Chemicals and reagents

MWCNT (multi-walled carbon nanotubes), H_2O_2, hydroquinone, ABTS (2.2′-azinobis [3-ethylbenzothiazoline-6-sulfonic acid]-diammonium salt), PBS (phosphate buffer saline) and epigallocatechin-3-gallate (EGCG, [(2*R*,3*R*)-5.7-dihydroxy-2-(3,4,5-trihydroxyphenyl)chroman-3-yl] 3,4,5-trihydroxybenzoate) were purchased from Sigma-Aldrich. Single layer graphene oxide (GO, diameter 1–5 μm; thickness 0.8–1.2 nm) was purchased from ACS Material LLC (Medford, MA, USA), which was synthesized by using the modified Hummer's method. Amino-modified DNA probe (DNA-P-141) and miRNAs (miR-141; miR-29b-1, sequences listed in Table 1) were supplied by Eurogentec (Belgium). Specific anti-RNAs were provided by Dr. D. Stollar, TUFTS University, Boston, MA. HRP-conjugated secondary antibodies (HRP-Ab2) were purchased from Abliance (France). 1-(3-dimethylaminopropyl)-3-ethylcarbodiimide hydrochloride (EDC, purity 98%) and N-hydroxysuccinimide (NHS, purity 98%) were from Alfa Aesar (Ward Hill, MA). Polyoxyethylenesorbitan monolaurate 20 (Tween20) and 2-(N-morpholino)ethanesulfonic (MES) buffer were from Sigma-Aldrich. Aqueous solutions were made with ultrapure (DI, 18 MΩ cm) water. Gold screen-printed electrodes (GSPE, 1.6 mm diameter) were formed Dropsens.

2.2. Methods and apparatus

2.2.1. Electrochemical measuring

For electrochemical experiments, a small (200 μL) one-compartment, three-electrode cell was used with an Autolab PGSTAT 30. The auxiliary electrode was screen-printed gold and the reference electrode was screen-printed silver. Cyclic voltammograms (CVs) and square wave voltammograms (SWVs) were recorded in PBS containing 4 mM hydroquinone and 3 mM H_2O_2. Before measurements, electrodes were incubated in 40 μL of this solution for 10 min. CVs were performed between +0.6 V and −0.6 V (vs. Ag/AgCl) at 50 mV s^{-1} scan rate. SWV were recorded between +0.4 V and −0.3 V (vs. Ag/AgCl), pulse height 50 mV, pulse width 50 ms, scan increment 2 mV, frequency 12.5 Hz. For each experiment, three independent electrodes were used, in order to establish error bars, reported on SWVs.

2.2.2. ELISA test

To validate electrochemical tests, ELISA experiments were performed under the same experimental conditions. 40 μL PBS containing 1 mM ABTS and 24.5 mM H_2O_2 were dropped on an electrode and let to incubate for 20 min at room temperature, then the optical density (OD) was read at 405 nm with a UV–vis Nanodrop apparatus.

Table 1
ODN probes and miRNA target sequences.

ODN name	Function (type)	Sequences
ODN-141-P	Probe (DNA)	5′ NH_2 – CCA TCT TTA CCA GAC AGT GTT A 3′
miR-141	Target (RNA)	3′ GGU AGA AAU GGU CUG UCA CAA U 5′
miR-29b-1	Target (RNA)	3′ UUG UGA CUA AAG UUU ACC ACG AU 5′

2.2.3. Characterizations

GO, reduced graphene oxide (RGO) and epigallocatechin-3-gallate (EGCG) were characterized by FT-IR and UV–vis. AFM samples were prepared by drop-casting the RGO suspensions on indium-tin oxide (ITO)-covered glass plates. Scanning Electron Microscopy (SEM) samples were prepared by drop-casting o-MWCNT/RGO suspensions on ITO plates.

2.2.4. Oxidized MWCNT (o-MWCNT) preparation

Multi-walled carbon nanotubes were oxidized by a 1:1 mixture of sulfuric acid and nitric acid at 90 °C for 1 h, then washed with distillated water until pH 7 and separated by centrifugation. The solid residue was then dried at 80 °C for 12 h. The resulting o-MWCNT was dispersed in DI water before use.

2.2.5. Reduced graphene oxide (RGO) preparation

24 mg of GO was dispersed in water under sonication for 30 min. 10 mg of EGCG was added to the GO dispersion then the mixture was heated up to 80 °C under stirring for 8 h. The suspension was cooled down to room temperature, filtered and washed with distillated water to obtain a black precipitate which was dispersed into water before use.

2.2.6. o-MWCNT/RGO/GSPE preparation

o-MWCNT and RGO were sonicated together (50% w/w) for 30 min at room temperature (r.t.) in water to obtain homogeneous dispersion. 10 μL of this dispersion was dropped on freshly cleaned gold screen-printed electrode and kept at r.t. to let water evaporate, leading to o-MWCNT/RGO/GSPE electrode. We used a quantity of material corresponding to 35 μg cm^{-2} of o-MWCNT/RGO composite.

2.2.7. DNA probe immobilization

o-MWCNT/RGO/GSPE were incubated in a solution containing 1 μM of amino-modified ODN probe (ODN-141-P) in 20 mM EDC +20 mM NHS in 0.1 M MES buffer at r.t., overnight. Then, electrodes were washed with 0.05% Tween20 in PBS to remove adsorbed ODN, leading to ODN/o-MWCNT/RGO/GSPE electrodes.

2.2.8. Hybridization assay

ODN-141-P/o-MWCNT/RGO/GSPE electrodes were incubated in PBS containing the miRNA target at 37 °C for 1 h then washed thrice with PBS, leading to miR-141/ODN-141-P/o-MWCNT/RGO/GSPE electrodes.

2.2.9. Complexation of anti-RNA.DNA antibody and HRP conjugated secondary antibody (Ab2-HRP)

miR-141/ODN-P-141/o-MWCNT/RGO/GSPE electrodes were immersed in PBS containing 100 nM of anti-RNA.DNA antibody, at r.t. for 1 h then washed thrice with 0.05% Tween20 in PBS. Next, the electrode was incubated in a solution containing 100 nM of Ab2-HRP for 30 min then washed thrice with 0.05% Tween20 in PBS, leading to Ab2-HRP/Ab1/miR-141/ODN-P-141/o-MWCNT/RGO/GSPE electrodes.

3. Results and discussion

3.1. o-MWCNT/RGO/GSPE electrodes

Graphene oxide was reduced by epigallocatechin gallate (EGCG, see structure in Supporting material, Fig. S1) to obtain water-soluble reduced graphene oxide (RGO). EGCG is known to be a very effective mild reducing agent for graphene and, in addition, presents π-conjugated structure which interacts with graphene sheets and helps disaggregation of graphene bundles to provide stable dispersions (Liao et al., 2011). Multiwall carbon nanotubes (MWCNTs) were modified following a protocol previously reported to obtain carboxyl-modified MWCNTs (o-MWCNT) (Thakur and Karak, 2012). RGO and o-MWCNT were dispersed in water and drop-casted on gold screen-printed electrodes (GSPE), to obtain o-MWCNT/RGO/GSPE electrodes. The idea is to use graphene-CNT hybrid with synergic properties of both CNT and graphene: RGO provides very high specific surface area while o-MWCNTs provide carboxyl groups for subsequent covalent coupling with amino-modified DNA probes.

For optical ELISA assays, the primary anti-RNA.DNA antibody (Ab1) was added to selectively bind miRNA.DNA hybrids; then, an HRP-conjugated secondary antibody (Ab2-HRP) was added to bind the primary antibody. Hydrogen peroxide (H_2O_2) and, typically, 2.2′-azino-bis(3-ethylbenzothiazoline-6-sulphonic acid) (reduced form of ABTS, colorless) were added as co-substrate and substrate, respectively; HRP catalyzed ABTS oxidation by hydrogen peroxide, turning it into a colored oxidized product that was detected spectrophotometrically. This was used as a reference technique, for validation of the electrochemical assays.

UV–vis spectra of GO, EGCG and RGO are depicted in Fig. S2. GO shows a peak at 234 nm and a shoulder at 303 nm. After reduction by EGCG, a peak appears at 269 nm, characteristic of RGO (Tran et al., 2013b). FTIR spectra are depicted in Fig. S3. GO (curve c) shows hydroxyl (O–H), carbonyl (H–C=O) and epoxide (–C–O–C–) groups. Bands at 3400 cm^{-1}, 1346 cm^{-1} and 1208 cm^{-1} are associated with stretching and deformation vibrations of O–H bond of –C–O–H (Ma et al., 2012) while bands at 1718 cm^{-1} and 1618 cm^{-1} are due to C=O of carboxyl group and C=C of aromatic rings, respectively. The band at 1059 cm^{-1} is attributed to C–O–C of epoxide group and C–O stretching (Ma et al., 2012; Liao et al., 2011; Thakur and Karak, 2012; Wang et al., 2011). After reduction by EGCG (curve b) these absorption bands decrease. Comparison with the EGCG spectrum (curve a) shows that EGCG on RGO is not detectable. Fig. S4 shows AFM pictures of RGO deposited on ITO plates, following the above-described protocol. It shows that RGO sheets have a thickness of about 2 nm, suggesting that some EGCG may be adsorbed on RGO sheets, even if not visible on FTIR spectrum. SEM pictures of o-MWCNT/RGO-modified ITO are shown in Fig. S5. They show a porous and homogeneous o-MWCNT/RGO layer on ITO, with o-MWCNT distributed between RGO sheets.

Modified and unmodified gold screen-printed electrodes (GSPE) were electrochemically characterized in deaerated PBS containing 4 mM hydroquinone, by cyclic voltammetry (CV, Fig. 1a) and square ware voltammetry (SWV, Fig. 1b). CVs of bare GSPE (dotted curve) present a couple of peaks situated at 0.67 V and −0.16 V (vs. SCE); ΔE_p is large, ca. 0.83 V. In the case of o-MWCNT/RGO/GSPE, the oxidation peak is situated at 0.13 V and the reduction peak at −0.05 V; ΔE_p is 0.18 V, which indicates that o-MWCNT/RGO facilitates electron transfer of hydroquinone/benzoquinone system. This reversibility appears even more clearly on SWV recorded for reduction of hydroquinone on bare GSPE (dotted curve) and o-MWCNT/RGO/GSPE (solid line, Fig. 1b).

3.2. miRNA immunodetection

Electrochemical measurements were carried out in a miniaturized electrochemical cell containing 200 μL of 0.1 M PBS+4 mM hydroquinone. SWVs are depicted in Fig. 2. Curve (a) corresponds to o-MWCNT/RGO/GSPE electrode in this medium, before probe grafting. It shows a strong reduction peak centered at 0.1 V with a faradic peak current of ca. 400 μA (baseline subtracted), which decreases down to 250 μA after DNA grafting (curve b) and hybridization with 1 nM of the complementary miR-141. This current decrease was not observed if EDC+NHS were not used

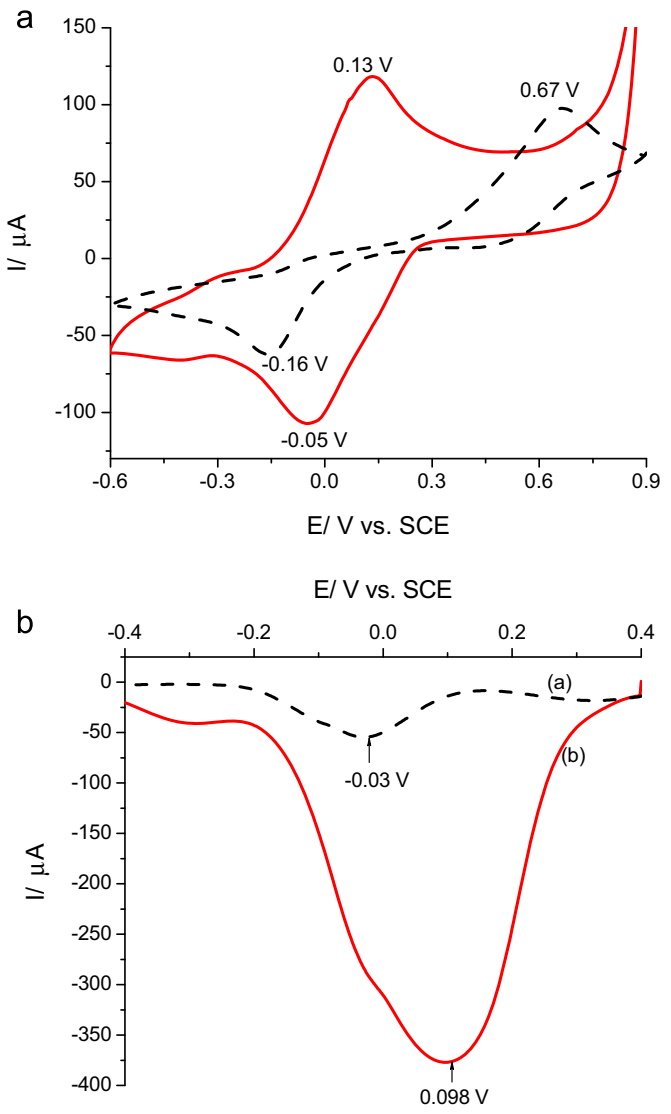

Fig. 1. (a) CVs and (b) SWVs of bare GSPE (dash) and o-MWCNT/RGO/GSPE (solid) in 0.1 M PBS+4 mM hydroquinone. Scan rate 50 mV s^{-1}.

for DNA grafting (result not shown). The peak current continues to decrease down to 150 μA after complexation with the primary antibody Ab1 then the secondary one HRP-Ab2 (curve c). This behavior could be attributed to steric hindrance from the antibodies, which hinder diffusion at the electrode interface (it was verified that the Q/H_2Q redox kinetics on such electrode are governed by diffusion, as CV's peak currents linearly depend on $v^{1/2}$ – see Fig. S6). However, after addition of 5 mM H_2O_2, the reduction peak increases to 320 μA (curve d), which is attributed to reduction of benzoquinone produced back to hydroquinone.

$$H_2O_2 + HRP_{red} \rightleftharpoons H_2O + HRP_{ox}$$
$$HRP_{ox} + H_2Q \rightleftharpoons HRP_{red} + BQ$$
$$BQ + 2e^- + 2H^+ \rightleftharpoons H_2Q$$

3.3. Selectivity and sensitivity

Under the same experimental conditions than for Fig. 2, other experiments were performed to demonstrate that the current increase is specifically due to the presence of HRP (Fig. 3). Ab1 was added but not HRP-Ab2 (curve a), neither Ab1 nor HRP-Ab2 was added (curve b), HRP-Ab2 was added but not Ab1 (curve c), then both Ab1 and HRP-Ab2 (curve d). As shown, HRP-Ab2, without previous addition of Ab1, leads to a current increase,

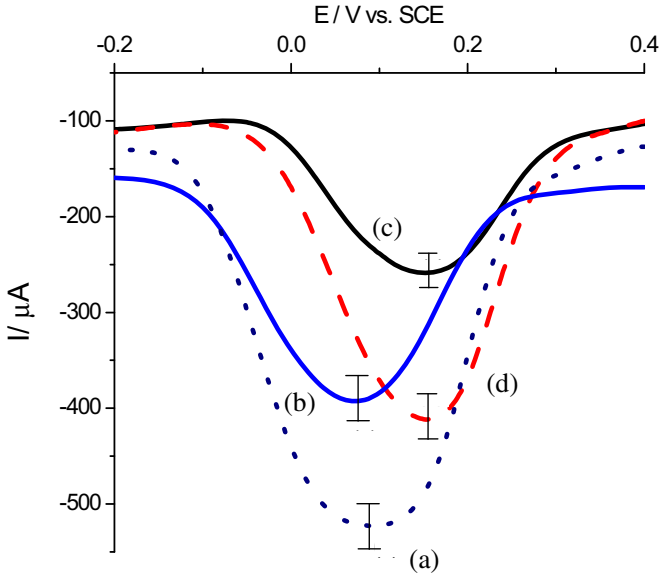

Fig. 2. SWV recorded for (a) o-MWCNT/RGO/GSPE; (b) same than (a), after immobilization of DNA probe; (c) same as (b), after hybridization with 1 nM of complementary target miRNA and (d) same as (c), after complexation with Ab/Ab2-HRP. Medium: PBS containing 4 mM hydroquinone without (a, b, c) and with (d) 5 mM H_2O_2.

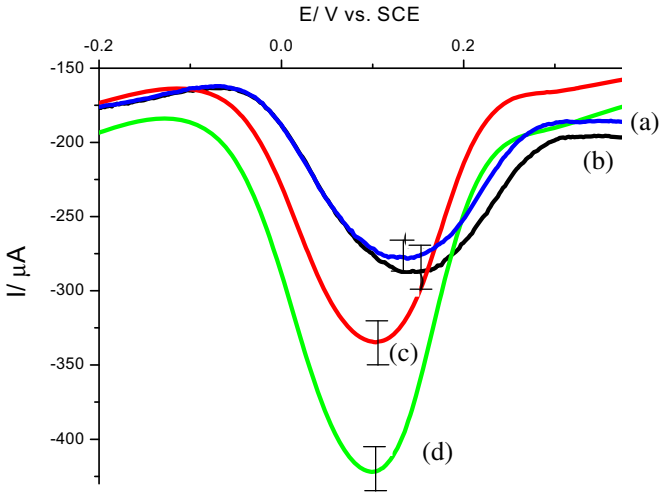

Fig. 3. SWVs recorded for (a) Ab1/miR-141/ODN-141-P/o-MWCNT/RGO/GSPE; (b) miR-141/ODN-141-P/o-MWCNT/RGO/GSPE; (c) HRP-Ab2/miR-141/ODN-141-P/o-MWCNT/RGO/GSPE (no Ab1) and (d) HRP-Ab2/Ab1/miR-141/ODN-141-P/o-MWCNT/RGO/GSPE . Medium: 5 mM. H_2O_2+4 mM hydroquinone in 0.1 M PBS. [miRNA]=1 nM. Incubation time: 10 min.

which is attributed to non-specific adsorption of the labeled secondary antibody. However, if the primary antibody is present, the current increase is significantly higher. Fig. S7 summarizes these results.

Sensitivity was investigated using various miR-141 concentrations within the range 10 fM–1 nM. SWVs are depicted in Fig. S8; the calibration curve is shown in Fig. 4. As shown, the peak current increases as a function of miR-141 concentration until it reaches saturation and decreases for concentrations above 10^{-10} M. Considering the standard deviation as well as the peak current obtained for blank experiments (around -190.6 ± 1.2 μA), one can estimate a limit of detection of ca. 30 fM.

To investigate selectivity, ODN-141-P/o-MWCNT/RGO/GSPE electrodes were hybridized with miR-141 (complementary target), miR-29b (non-complementary target) or without any target

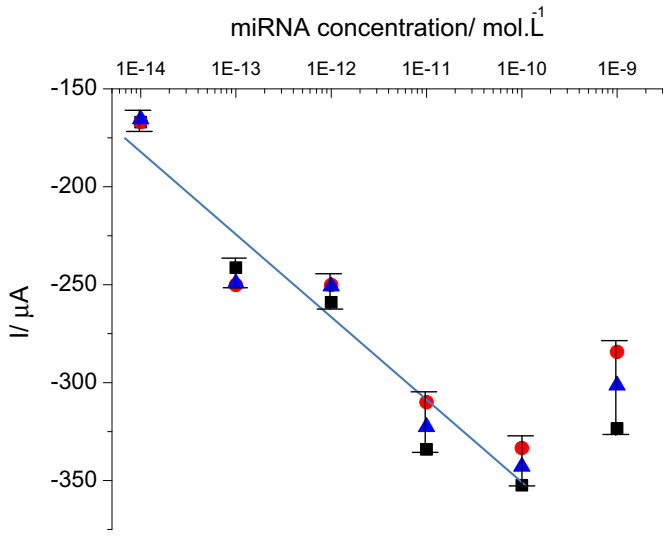

Fig. 4. Calibration curve in a dynamic range from 10 fM to 1 nM for miR-141 detection, obtained from results of Fig. S9 (from three independent electrodes).

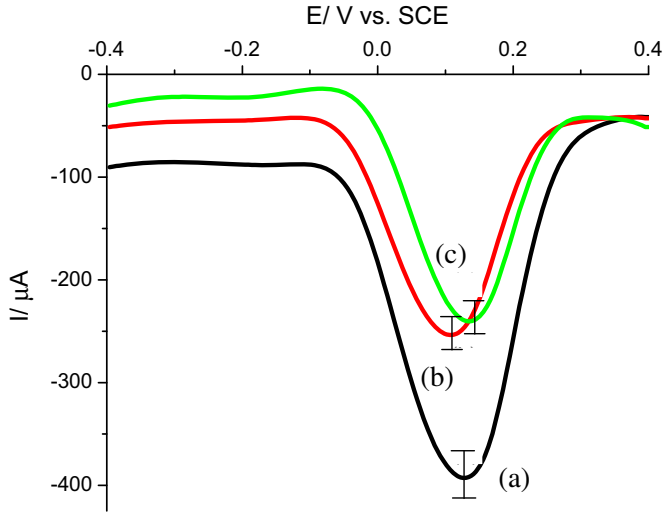

Fig. 5. SWVs of HRP-Ab2/Ab1/miRNA/DNA/o-MWCNT/RGO/GSPE electrodes, for (a) 10 nM of complementary miR-141 target; (b) 10 nM of non-complementary miR-29b target and (c) blank sample (no MiR). Medium: 5 mM H_2O_2+4 mM hydroquinone in PBS. Incubation time: 10 min.

(blank), then Ab1 and HRP-Ab2 were added. SWV were recorded in 0.1 M PBS containing 4 mM hydroquinone+5 mM H_2O_2 (Fig. 5). Reduction current for the blank sample (curve c) and non-complementary target (curve b) are almost the same while the reduction current corresponding to the complementary target is significantly higher (curve a).

Classical optical ELISA tests were performed to confirm these electrochemical experiments (Fig. 6). Three controls were used (one blank, and two non-complementary miRNAs). As shown, ELISA experiments confirm the selectivity of the anti-RNA.DNA antibody recognition, and corroborate well electrochemical experiments.

4. Conclusion

In this study, we present a novel approach to prepare carbon nanotubes/reduced graphene oxide-modified gold screen-printed electrodes, for electrochemical detection of miRNA. This material

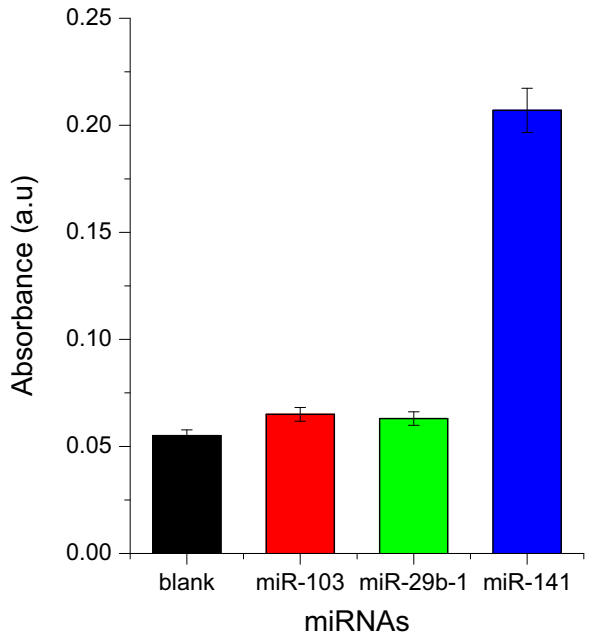

Fig. 6. Optical densities measured at 405 nm for HRP-Ab2/Ab1/miRNA/DNA/o-MWCNT/RGO/GSPE electrodes tested under ELISA conditions (see Section 2). Blank corresponds to no miR target; miR-103 is a non-complementary miRNA having the sequence 3′AGU AUC GGG ACA UGU UAC GAC GA 5′.

forms a conducting interpenetrated network which increases the electroactive area while decreasing electrical resistance of working electrodes and carries chemical groups useful for subsequent grafting of functional (bio)molecules. In addition, the use of enzymatic amplification gives very high current densities, which makes this approach applicable for very small working electrode areas. The strategy, in combination with an original immunological approach using antibodies directed to DNA.RNA hybrids allows us to design selective and sensitive miRNA sensors with detection limit in the fM range.

Acknowledgments

H.V. Tran thanks the University of Sciences and Technology of Hanoi (USTH) for a PhD grant (VIED- MOET Grant 911). The authors thank Sorbonne Paris Cité for financial support through an Interdisciplinary Grant ANR-11-IDEX-05-02 "*Once upon a tooth*". L. Huy Nguyen thanks the NAFOSTED (code:104.03-2011.58) for a research training course at the laboratory ITODYS.

Appendix A. Supporting material

Supplementary data associated with this article can be found in the online version at 10.1016/j.bios.2014.06.014.

References

Cai, Z., Song, Y., Wu, Y., Zhu, Z., Yang, C.J., Chen, X., 2013. Biosens. Bioelectron. 41, 783–788.
Chen, D., Feng, H., Li, J., 2012. Chem. Rev 112, 6027–6053.
Cui, L., Lin, X.Y., Lin, N.H., Song, Y.L., Zhu, Z., Chen, X., Yang, C.J., 2012. Chem. Commun. 48, 194–196.
Dong, H., Ding, L., Yan, F., Ji, H., Ju, H., 2011. Biomaterials 32, 3875–3882.
Dong, H., Jin, S., Ju, H., Hao, K., Xu, L.P., Lu, H., Zhang, X., 2012b. Anal. Chem. 84, 8670–8674.
Dong, H., Lei, J., Ju, H., Zhi, F., Wang, H., Guo, W., Zhu, Z., Yan, F., 2012c. Angew. Chem. Int. Ed. 51, 4607–4612.

Dong, H., Zhang, J., Ju, H., Lu, H., Wang, S., Jin, S., Hao, K., Du, H., Zhang, X., 2012a. Anal. Chem. 84, 4587–4593.
Dreyer, D.R., Park, S., Bielawski, C.W., Ruoff, R.S., 2010. Chem. Soc. Rev. 39, 228–240.
Fan, Y., Chen, X., Trigg, A.D., Tung, C., Kong, J., Gao, Z., 2007. J. Am. Chem. Soc. 129, 5437–5443.
Fang, S., Lee, H.J., Wark, A.W., Corn, R.M., 2006. J. Am. Chem. Soc. 128, 14044–14046.
Fang, Z., Soleymani, L., Pampalakis, G., Yoshimoto, M., Squire, J.A., Sargent, E.H., Kelley, S.O., 2009. ACS Nano 3, 3207–3213.
Feng, L., Wu, L., Qu, X., 2013. Adv. Mater. 25, 168–186.
Feng, L., Wu, L., Wang, J., Ren, J., Miyoshi, D., Sugimoto, N., Qu, X., 2012. Adv. Mater. 24, 125–131.
Fliss, I., St-Laurent, M., Emond, E., Simard, R.E., Lemieux, R., Ettriki, A., Pandian, S., 1995. Appl. Microbiol. Biotechnol. 43, 717–724.
Gao, Z., Deng, H., Shen, W., Ren, Y., 2013. Anal. Chem. 85, 1624–1630.
Georgakilas, V., Otyepka, M., Bourlinos, A.B., Chandra, V., Kim, N., Kemp, K.C., Hobza, P., Zboril, R., Kim, K.S., 2012. Chem. Rev. 112, 6156–6214.
Hu, Y., Wang, K., Zhang, Q., Li, F., Wu, T., Niu, L., 2012. Biomaterials 33, 1097–1106.
Huang, X., Zeng, Z., Fan, Z., Liu, J., Zhang, H., 2012. Adv. Mater. 24, 5979–6004.
Labib, M., Khan, N., Ghobadloo, S.M., Cheng, J., Pezacki, J.P., Berezovski, M.V., 2013. J. Am. Chem. Soc. 135, 3027–3038.
Liao, R., Tang, Z., Lei, Y., Guo, B., 2011. J. Phys. Chem. C 115, 20740–20746.
Ma, H.L., Zhang, H.B., Hu, Q.H., Li, W.J., Jiang, Z.G., Yu, Z.Z., Dasari, A., 2012. ACS Appl. Mater. Interfaces 4, 1948–1953.
Peng, Y., Yi, G., Gao, Z., 2010. Chem. Commun. 46, 9131–9133.
Qavi, A.J., Kindt, J.T., Gleeson, M.A., Bailey, R.C., 2011. Anal. Chem. 83, 5949–5956.
Ramnani, P., Gao, Y., Ozsoz, M., Mulchandani, A., 2013. Anal. Chem. 85, 8061–8064.
Roy, S., Soh, J.H., Gao, Z., 2011. Lab Chip 11, 1886–1894.
Rudkin, G.T., Stollar, B.D., 1977. Nature 265, 472–473.
Sípová, H., Zhang, S., Dudley, A.M., Galas, D., Wang, K., Homola, J., 2010. Anal. Chem 82, 10110–10115.
Thakur, S., Karak, N., 2012. Carbon 50, 5331–5339.
Tran, H.V., Piro, B., Reisberg, S., Anquetin, G., Duc, H.T., Pham, M.C., 2014. Anal. Bioanal. Chem. 406, 1241–1244.
Tran, H.V., Piro, B., Reisberg, S., Duc, H.T., Pham, M.C., 2013a. Anal. Chem. 85, 8469–8474.
Tran, H.V., Piro, B., Reisberg, S., Tran, L.D., Duc, H.T., Pham, M.C., 2013b. Biosens. Bioelectron. 49, 164–169.
Wang, Y., Shi, Z., Yin, J., 2011. ACS Appl. Mater. Interfaces 3, 1127–1133.
Wu, L., Wang, J., Feng, L., Ren, J., Wei, W., Qu, X., 2012. Adv. Mater. 24, 2447–2452.
Yang, H., Hui, A., Pampalakis, G., Soleymani, L., Liu, F., Sargent, E.H., Kelley, S.O., 2009. Angew. Chem. Int. Ed. 48, 8461–8464.
Yin, H.S., Zhou, Y.L., Zhang, H.X., Meng, X.M., 2012. Biosens. Bioelectron. 33, 247–253.
Yoshichika, K., Stollar, B.D., 1982. Mol. Immunol. 19, 413–420.
Zhang, G.J., Chua, J.H., Chee, R.E., Agarwal, A., Wong, S.M., 2009. Biosens. Bioelectron. 24, 2504–2508.